



日本原子力研究開発機構機関リポジトリ
Japan Atomic Energy Agency Institutional Repository

Title	Nuclear quantum effects of light and heavy water studied by all-electron first principles path integral simulations
Author(s)	Machida Masahiko, Kato Koichiro, Shiga Motoyuki
Citation	Journal of Chemical Physics, 148(10), p.102324_1-102324_11
Text Version	Publisher's Version
URL	https://jopss.jaea.go.jp/search/servlet/search?5061297
DOI	https://doi.org/10.1063/1.5000091
Right	<p>This article may be downloaded for personal use only. Any other use requires prior permission of the author and the American Institute of Physics.</p> <p>The following article appeared in Journal of Chemical Physics and may be found at https://doi.org/10.1063/1.5000091.</p>

Nuclear quantum effects of light and heavy water studied by all-electron first principles path integral simulations

Masahiko Machida, Koichiro Kato, and Motoyuki Shiga

Citation: *The Journal of Chemical Physics* **148**, 102324 (2018);

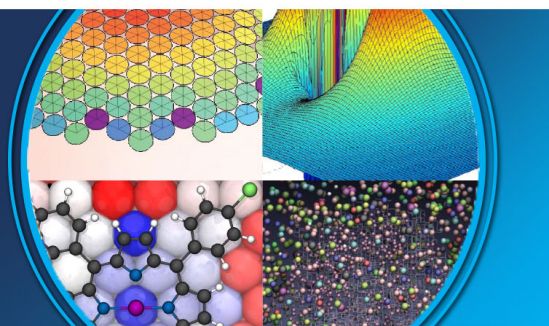
View online: <https://doi.org/10.1063/1.5000091>

View Table of Contents: <http://aip.scitation.org/toc/jcp/148/10>

Published by the [American Institute of Physics](#)

AIP | The Journal of
Chemical Physics

PERSPECTIVES



Nuclear quantum effects of light and heavy water studied by all-electron first principles path integral simulations

Masahiko Machida,¹ Koichiro Kato,² and Motoyuki Shiga¹

¹CCSE, Japan Atomic Energy Agency (JAEA), 178-4-4, Wakashiba, Kashiwa, Chiba 277-0871, Japan

²Mizuho Information and Research Institute, Inc., 2-3, Kandanishiki-cho, Chiyoda-ku, Tokyo 101-8443, Japan

(Received 14 August 2017; accepted 8 November 2017; published online 5 December 2017)

The isotopologs of liquid water, H₂O, D₂O, and T₂O, are studied systematically by first principles PIMD simulations, in which the whole entity of the electrons and nuclei are treated quantum mechanically. The simulation results are in reasonable agreement with available experimental data on isotope effects, in particular, on the peak shift in the radial distributions of H₂O and D₂O and the shift in the evaporation energies. It is found that, due to differences in nuclear quantum effects, the H atoms in the OH bonds more easily access the dissociative region up to the hydrogen bond center than the D (T) atoms in the OD (OT) bonds. The accuracy and limitation in the use of the current density-functional-theory-based first principles PIMD simulations are also discussed. It is argued that the inclusion of the dispersion correction or relevant improvements in the density functionals are required for the quantitative estimation of isotope effects. *Published by AIP Publishing.* <https://doi.org/10.1063/1.5000091>

I. INTRODUCTION

Understanding the hydrogen-bonded structure of liquid water has been a long-standing topic of general interest in chemical physics due to the ubiquity of water. In recent years, the structure of liquid water has been frequently studied by first principles or *ab initio* molecular dynamics (MD) simulations owing to computational and methodological advances.^{1–21} Molecular interactions are computed from electronic structure calculations on the fly along the molecular trajectory. Such simulations, without the use of any empirical parameters, enabled the direct comparison between theory and experiment. Much effort has been devoted to improve the quality of the simulations, but complete agreement has not been reached yet with respect to the true structure of water. In fact, it has been reported that density functional theory (DFT) calculations tend to promote overstructuring of liquid water, which results in a melting point higher than in reality.^{22–24} As the fundamental error in the simulations would be from the electron correlation issue, elaborations have been made to the choice of exchange-correlation functionals (for a recent review, see, e.g., Ref. 2), van der Waals corrections^{9,13,14,25–28} (for a recent review, see also, e.g., Ref. 2), or post Hartree-Fock theories^{13,17–19,29,30} used instead. Meanwhile other errors may arise from sampling issues,^{31,32} small system sizes,^{6,31} the choice of pseudopotentials (see, e.g., Ref. 33), the basis functions,³⁴ wavefunction optimizations, etc. (for a recent review, see also, e.g., Ref. 2). Investigations are still under way on these topics.

In the present paper, our main focus is on the nuclear quantum effects (NQEs) that lead to differences between the structures of light and heavy water. In standard first principles MD simulations, it is assumed that the atoms (nuclei) are classical particles that obey classical statistics. One of the important outcomes of classical statistics is that the atomic mass does

not affect thermodynamical properties, such as the structures, energies, free energies and their derivatives, etc. However this is clearly a theoretical drawback since it is experimentally evident that the thermodynamics are different under isotopic substitution. Since it is known that the Born-Oppenheimer approximation can accurately describe the potential energy of the electronic ground state, isotope effects on the thermodynamics are consequences of nuclear quantum effects. Therefore nuclear quantum effects play a vital role in distinguishing the properties of light and heavy water. Conversely the thermodynamic changes that occur with respect to the deuteration and tritiation of water are a sign that the quantum nature of the light proton is suppressed by the heavier deuteron or triton replacements.

One of the useful approaches to account for nuclear quantum effects is path integral molecular dynamics (PIMD), which is a general simulation method based on Feynman's imaginary-time path integral (PI) formulation of quantum statistical mechanics.^{35,36} The PI theory within the second-order Suzuki-Trotter expansion establishes an isomorphism between the quantum statistics of a particle and the classical statistics of a ring polymer coupled by harmonic springs.³⁷ Accordingly the quantum statistics for a system composed of many atoms can be obtained from the classical ensemble generated by the molecular dynamics simulation of a system of many ring polymers.³⁸ The method can be generalized as first principles or *ab initio* PIMD when combined with corresponding electronic structure calculations at a given level of theory.^{39–42} The nuclei and the electrons involved in the electronic structure calculations are thereby treated quantum mechanically, and all entities can be considered fully in first principles PIMD based on all-electron calculations.

A first principles PIMD simulation of liquid water was first reported by Chen, Ivanov, Klein, and Parrinello in 2003, based on the Car-Parrinello approach for a system of

64 water molecules [with the Becke-Lee-Yang-Parr (BLYP) exchange-correlation functional, norm-conserving pseudopotential, and 16 beads].²¹ Interestingly they reported that the structure of H₂O is almost the same as D₂O even in the presence of simulated nuclear quantum effects. The first peak of the oxygen-oxygen radial distribution of D₂O was slightly *higher* than that of H₂O, but this was in contrast to the results of path integral simulations using force fields based on empirical modeling^{43,44} and experiment.⁴⁵ In 2008, another first principles PIMD simulation of liquid water by Morrone and Car based on the Car-Parrinello approach for a system of 64 water molecules (with the BLYP exchange-correlation functional, Troullier-Martins norm-conserving pseudopotential, and 32 replicas) found that nuclear quantum effects do significantly soften the structure.⁴⁶ The first peak of the oxygen-oxygen radial distribution from the PIMD simulation of H₂O is *lower* than from the MD simulations of H₂O. Thereafter first principles PIMD simulations were used to study the structure of liquid H₂O, the structure of H₂O and D₂O in the liquid-vapor interface,^{47,48} and the fractionation ratio of H₂O and D₂O of liquid and vapor.^{49,50} In recent first principles PIMD simulations of liquid H₂O, the focus was on the nuclear quantum effect on the hydrogen bond structure and its impact on the electronic structure,^{19,20} etc. However “on-the-fly” first principles PIMD simulations on the structural isotope effect of H₂O and D₂O in the bulk liquid phase have not been presented since the first report in 2003.

In this paper, we report first principles PIMD simulations of light and heavy water in a systematic manner as follows. Our focus will be on comparing the hydrogen-bonded structures of H₂O, D₂O, and T₂O in the liquid state at room temperature. For the first time, the radial distributions of H₂O and D₂O from first principles PIMD simulations are compared against experimental data.^{45,51,52} Furthermore a hydrogen-bonded analysis of these isotopologs is presented, following the suggestions of Ceriotti, Cuny, Parrinello, and Manolopoulos.⁵³ We use an all-electron calculation based on the projector augmented wave (PAW) method in which the valence orbitals are kept orthogonal to the core orbitals.⁵⁴ This is in contrast to many of the previous PIMD simulations in which only the valence orbitals are explicitly solved based on the pseudopotential method. In addition, the path integral sampling is conducted directly using the conventional Suzuki-Trotter scheme without any approximations. All the electrons and nuclei are thereby treated quantum mechanically based on first principles. The important assumptions are simply the Born-Oppenheimer approximation, the density functional (BLYP-D2 in the present study), and the system size (64 water molecules). The impact of the D2 dispersion correction is studied systematically for the first time in the presence of the nuclear quantum effect for H₂O, D₂O, and T₂O.

To our knowledge, this is the first study of liquid T₂O using first principles simulations. Apart from the viewpoint of basic science, the chemical properties of tritiated water are important data in the context of the separation of nuclear waste and the impact on environment. In particular, for the contaminated water generated since the 2011 Fukushima nuclear power plant accident, it is tritium that has not been still separated due to its high expense and low efficiency. To develop a new

tritium separation technique using nanostructured materials, a contribution from computational science is currently required, see, e.g., Refs. 55 and 56.

II. METHOD

In this work, we carried out first principles path integral molecular dynamics (PIMD) calculations of H₂O, D₂O, and T₂O in the liquid and gas phases. We also carried out first principles molecular dynamics (MD) calculations of H₂O in the liquid and gas phases to study the cases without the nuclear quantum effect. For convenience, the MD and PIMD calculations are hereafter called the classical and quantum simulations, respectively.

All the calculations were undertaken using a combination of the PIMD code,⁵⁷ which is capable of path integral molecular dynamics simulations, and the VASP code,^{58–62} which enables calculation of the electronic structure based on PAW method allowing for hierarchically parallel computation.⁶³ The electronic structure calculations are based on density functional theory with the Becke-Lee-Yang-Parr (BLYP) exchange^{64,65} correlation functional with Grimme’s D2 van der Waals correction.⁶⁶ The plane wave basis functions were employed with a cutoff at 400 eV. Only the Γ -point of the Brillouin zone was computed.

The quantum and classical simulations were carried out based on the Born-Oppenheimer scheme where the self-consistent-field (SCF) convergence criteria was set to be 1.0×10^{-5} eV. For the liquid phase, the system was composed of 64 water molecules in a cubic box with the side length of 12.417 Å, which amounts to 1.00 g/cm³ in the case of H₂O, with periodic boundary conditions applied. For the gas phase, the system was composed of one water molecule in the cubic box of the same size. The temperature was controlled at 300 K with Nosé-Hoover chain (NHC) thermostats^{67–69} massively attached to each degree of freedom to efficiently generate the NVT ensemble. An imaginary time slice of the second-order Suzuki-Trotter expansion (the number of beads) of $P = 16$ was employed for all the quantum simulations. Two independent studies have found earlier that the use of $P = 16$ is on the edge of convergence for path integral simulations of water at room temperature with respect to the energies⁷⁰ and the interatomic distributions.⁷¹ The quantum and classical simulations were 21 ps each, of which 6 ps and 15 ps were taken for the equilibration and the production runs, respectively. The statistical convergence of the results was checked by the block averages. We provide the results along with the error estimates from the blocks of two halves of the production runs. For efficient sampling, the simulations were launched from the equilibrated structures of preliminary simulations using an empirical force field. The time step size was chosen to be $\Delta t = 0.25, 0.35,$ and 0.43 fs for H₂O, D₂O, and T₂O, respectively, which are sufficiently shorter than the respective time scales of molecular vibrations. The multiple time scale technique with the reversible reference system propagator algorithm (RESPA) was employed to integrate the NHC thermostats five times per Δt .⁷² In the quantum simulations, the equation of motion was solved in the normal mode representation to enable an efficient sampling of beads having stiff harmonic interactions.⁷³ Using

this setting, it was confirmed that the simulations conserve energy.

We have used two parallel computer systems (BX900 with 1024 cores and ICE-X with 1536 cores) in JAEA. A single step of PIMD calculations required 26 s on BX900 and 14 s on ICE-X. We note that the present PIMD simulations are based on the explicit Suzuki-Trotter expansion, the Born-Oppenheimer scheme, and the all-electron PAW method, which is computationally more expensive than most of the previous first principles calculations of liquid water.²

In obtained MD step data, for convenience, the hydrogen bond is defined following the convention by Luzar and Chandler.⁷⁴ Two water molecules were assumed to be hydrogen bonded when the intermolecular O \cdots O distance was less than 3.5 Å and simultaneously one of the O \cdots H-O angles was less than 30°.

III. RESULTS AND DISCUSSIONS

A. Hydrogen-bonded structures

Snapshots from the present classical and quantum simulations are shown in Fig. 1. In the classical simulations, the atomic nuclei were described as classical point particles [Fig. 1(a)]. Since the classical canonical ensemble generated in the classical simulation is identical under isotopic substitutions, the molecular structures and the energies obtained should be identical for D₂O and T₂O. Therefore all the statistical results will also be identical. In the quantum simulations shown in Figs. 1(b)–1(d), the quantum nuclei are described by sets of beads, i.e., members of the ring polymer in the

imaginary-time path integral representation. The spatial spread of the beads is due to the quantum fluctuations arising from the uncertainty principle. The quantum canonical ensembles generated by the quantum simulations reflect the effects of nuclear mass and thus the isotopic effects on the molecular structure and energies, in contrast to the classical simulation. The quantum fluctuations of H₂O are larger than those for D₂O and T₂O because H is stronger than D and T in quantum nature. However quantum fluctuations are not negligible even for the heaviest T₂O, as can be judged visually by comparing Figs. 1(a) and 1(d).

B. Thermodynamic averages

In Table I, we list the thermal averages of the OH bond distance, $\langle r_{\text{OH}} \rangle$, and the HOH bond angle, $\langle \theta_{\text{HOH}} \rangle$, for liquid and gaseous water, and the evaporation energy for liquid water, ΔU , obtained from the classical and quantum simulations along with the ranges of statistical error. The results are compared with those from the previous path integral simulations based on *ab initio* second-order Møller-Plesset perturbation (MP2) theory⁷⁵ and the empirical SPC/F2 model.⁷⁶ Comparisons are also drawn with available experimental data.^{77,78}

Comparing the classical and quantum simulations, we find that the nuclear quantum effect results in a stretching of the $\langle r_{\text{OH}} \rangle$ distance from 0.995 Å to 1.014 Å in liquid water. The $\langle r_{\text{OH}} \rangle$ distances for liquid D₂O and T₂O are within this range. The $\langle r_{\text{OH}} \rangle$ distance in liquid water is longer than that in gaseous water because of the hydrogen bonding. However the nuclear quantum effect itself is mainly inherited from gaseous water,

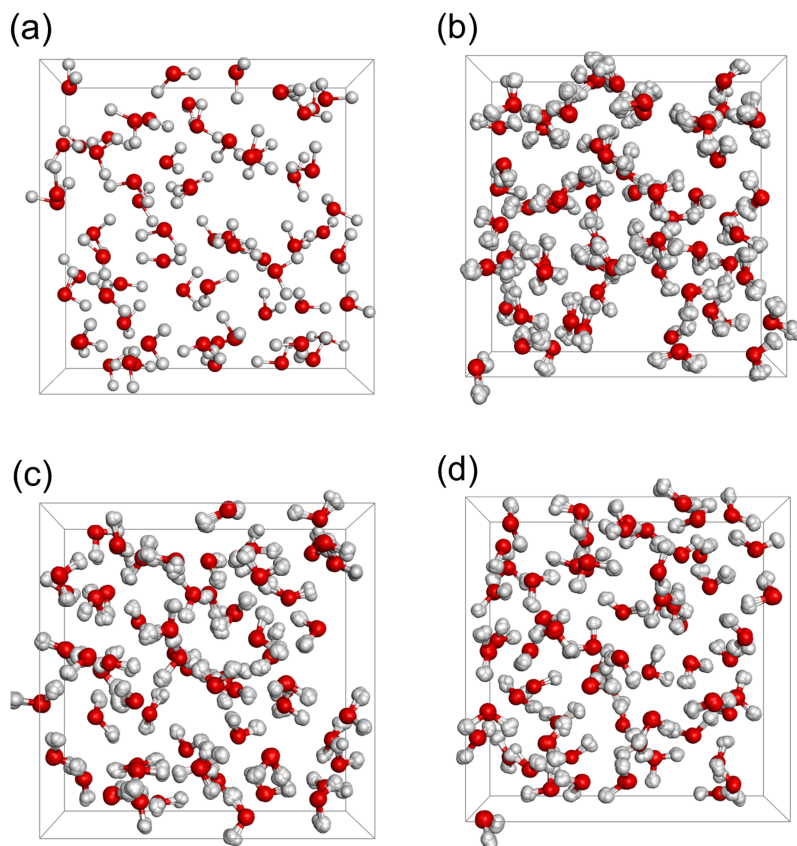


FIG. 1. Snapshots from the simulations of liquid water. (a) Classical simulation of H₂O and quantum simulations of (b) H₂O, (c) D₂O, and (d) T₂O. The red and white circles represent nuclear positions (nuclear bead positions) of oxygen and hydrogen, respectively, in classical (quantum) simulations.

TABLE I. Bond lengths, bond angles, and evaporation energies.^a

Method	System	$\langle r_{\text{OH}} \rangle$ (Å)	$\langle \theta_{\text{HOH}} \rangle$ (deg)	ΔU (kcal/mol)
Classical (PAW/BLYP-D2) ^b	Liquid H ₂ O	0.995 ± 0.000	106.5 ± 0.09	11.86 ± 0.17
	Gaseous H ₂ O	0.978 ± 0.000	105.0 ± 0.06	
Quantum (PAW/BLYP-D2) ^b	Liquid H ₂ O	1.014 ± 0.000	106.5 ± 0.08	11.17 ± 0.10
	Liquid D ₂ O	1.008 ± 0.000	106.3 ± 0.00	11.53 ± 0.10
	Liquid T ₂ O	1.006 ± 0.001	106.6 ± 0.14	11.78 ± 0.08
	Gaseous H ₂ O	0.992 ± 0.000	104.7 ± 0.08	
	Gaseous D ₂ O	0.989 ± 0.000	104.7 ± 0.05	
	Gaseous T ₂ O	0.985 ± 0.000	104.8 ± 0.22	
Classical (MP2) ^c	Gaseous H ₂ O	0.966	105.4	
Quantum (MP2) ^c	Gaseous H ₂ O	0.981	105.0	
	Gaseous D ₂ O	0.976	105.0	
Classical (SPC/F2) ^d	Liquid H ₂ O	1.021	104.1	
Quantum (SPC/F2) ^d	Liquid H ₂ O	1.019	104.9	9.7
	Liquid D ₂ O	1.020	104.6	10.3
Expt. ^e	Liquid H ₂ O			10.0
	Liquid D ₂ O			10.4
Expt. ^f	Gaseous H ₂ O	0.9743	104.52	

^aIf the error is represented as all digits being filled with zero, e.g., 0.000 and 0.00, it means that the error is less than the reported precision.

^bThis work.

^cPath integral simulations based on *ab initio* MP2 theory.⁷⁵

^dPath integral simulations based on empirical SPC/F2 model.⁷⁶

^eValue derived from the experimental vaporization enthalpy, ΔH ,⁷⁸ with the ideal-gas approximation, $\Delta U = \Delta H - RT$.

^fReference 77 and references therein.

as it stretches the $\langle r_{\text{OH}} \rangle$ distance from 0.978 Å to 0.992 Å. The distances for gaseous D₂O and T₂O are within this range. This result is reasonable since the same trend was found in the previous *ab initio* MP2 simulations of gaseous water, in which the $\langle r_{\text{OH}} \rangle$ distance was stretched from 0.966 Å to 0.976 Å by the nuclear quantum effect. Therefore changes in the $\langle r_{\text{OH}} \rangle$ distance from gas to liquid are mainly due to the anharmonic nature of the intramolecular OH bond in liquid states affected by quantum fluctuations, in particular, the zero point vibration. In fact, the nuclear quantum effect on the $\langle r_{\text{OH}} \rangle$ distance was found to be small in previous empirical SPC/F2 simulations where the OH bonds were modeled as harmonic springs.

The influence of the nuclear quantum effect on the $\langle \theta_{\text{HOH}} \rangle$ angle is small, both in gaseous water and liquid water. On the other hand, the hydrogen bonding does have a substantial effect on the $\langle \theta_{\text{HOH}} \rangle$ angle. In our quantum simulations of H₂O, the $\langle \theta_{\text{HOH}} \rangle$ angle is found to shift from 104.7° in the gaseous state to 106.5° in the liquid state.

In contrast to the classical case, in the quantum simulations, the evaporation energy of liquid water can be distinguished between the isotopologs, H₂O, D₂O, and T₂O. The difference of evaporation energies between liquid D₂O and H₂O is estimated at 11.53 – 11.17 = 0.36 kcal/mol, which agrees well with the experimental data, 10.4 – 10.0 = 0.4 kcal/mol. The difference of evaporation energies should be relevant to the difference of boiling points between H₂O (100.0 °C at 1 atm) and D₂O (101.4 °C), indicating that the former evaporates with less energy than the latter. Similarly the quantum simulations predict that the evaporation energy of liquid T₂O is 0.25 kcal/mol higher than liquid D₂O and 0.61 kcal/mol higher than liquid H₂O.

Although the shift for different isotopologs is reasonable, we find that the absolute values of the evaporation energies do not agree well between our simulation (11.2 kcal/mol for H₂O) and experiment (10.0 kcal/mol). This overestimation is one of the limitations of the simulation method. It is presumably related to the error arising from the estimate of the electron

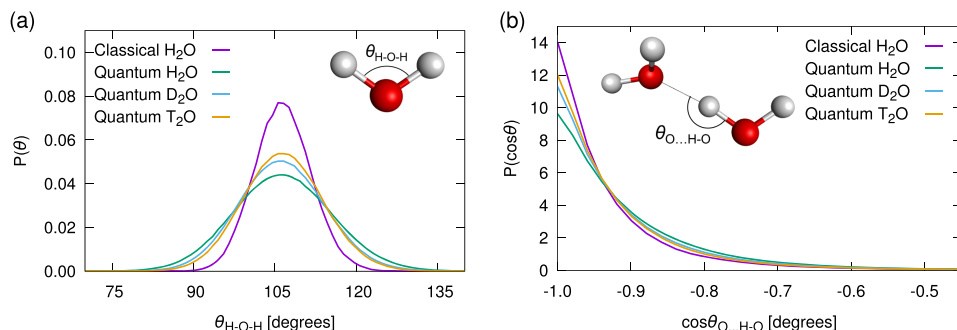


FIG. 2. Distributions of (a) the HOH bond angle of the water molecule, θ_{HOH} , and (b) the O...H-O angle, $\theta_{\text{O}\cdots\text{H}-\text{O}}$, of hydrogen-bonded pairs of water molecules in the liquid phase. The definitions of the angles θ_{HOH} and $\theta_{\text{O}\cdots\text{H}-\text{O}}$ are described in the figure. The results are shown for the classical simulation of H₂O (violet) and the quantum simulations of H₂O (green), D₂O (blue), and T₂O (orange).

correlation, in light of the report that the structure of water is highly dependent on the type of DFT functional.² In fact, the $\langle r_{\text{OH}} \rangle$ distance of gaseous H₂O obtained in the present PAW/BLYP-D2 quantum simulation, 0.992 Å, is larger than that obtained from *ab initio* MP2 quantum simulation, 0.981 Å, as well as the experimental value, 0.9743 Å. The error can be traced back to the optimized structure of the gaseous H₂O molecule, i.e., the equilibrium OH bond length is 0.974 Å in the PAW/BLYP-D2 method while the experimental value is 0.9572 Å.⁷⁷ The overestimation of the OH bond length, and thus the dipole moment of water, may be one of the factors that results in overly strong hydrogen bonding. This issue will be discussed again when examining the radial distribution functions shown in Figs. 4–6.

C. Bond distributions

Although the nuclear quantum effect does not have a significant influence on the averages of the HOH bond angle θ_{HOH} , it does have a strong influence on the fluctuations of θ_{HOH} . In Fig. 2(a), it is shown that the θ_{HOH} bond angle distribution is broadest in the H₂O quantum simulation, followed by the D₂O and T₂O quantum simulations. More importantly, HOH bending has an impact on the linearity of the hydrogen bond. The distribution of the $\theta_{\text{O} \dots \text{H}-\text{O}}$ angle for a pair of hydrogen-bonded water molecules follows the same pattern as above—the quantum H₂O simulation is broadest, followed by D₂O and T₂O [Fig. 2(b)]. This result is reasonable in that the hydrogen bond distortion comes from mainly the bending motion, the libration/rotation or their combinations, and that the bending modes are of higher frequency than the libration/rotation modes and thus they are stronger in quantum nature.

In Fig. 3, we show the hydrogen bond probability, $P(n)$, which was obtained by counting the number of hydrogen bonds per oxygen atom. The probability $P(2)$ is smaller and the

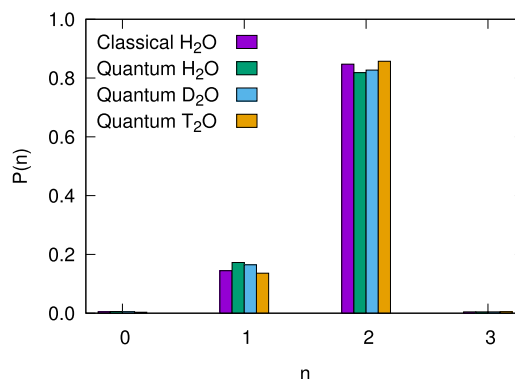


FIG. 3. Probability, $P(n)$, of finding the number of hydrogen bonds, n , connected to an oxygen atom as the H-bond acceptor in the classical simulation of H₂O (violet) and the quantum simulations of H₂O (green), D₂O (blue), and T₂O (orange).

probability $P(1)$ is larger, again, in the order H₂O, D₂O, and then T₂O. This means that the nuclear quantum effect has the tendency not only to distort but also to break one of the two hydrogen bonds that form for the oxygen atom.

D. Radial distributions

The radial distributions obtained from the classical and quantum simulations are displayed in Figs. 4–6, along with the experimental results from Refs. 45, 51, and 52. The experimental data were collected from neutron diffractions and X-ray diffractions for oxygen-oxygen, oxygen-hydrogen, and hydrogen-hydrogen radial distributions of H₂O and D₂O. The peak positions and peak heights of these radial distributions are summarized in Table II along with the ranges of statistical error. From Figs. 4–6 and Table II, we can see that the peak positions are in good agreement between the simulations and the experiments. However the agreement in the absolute value of the peak heights is not as good. The strong undulation of the

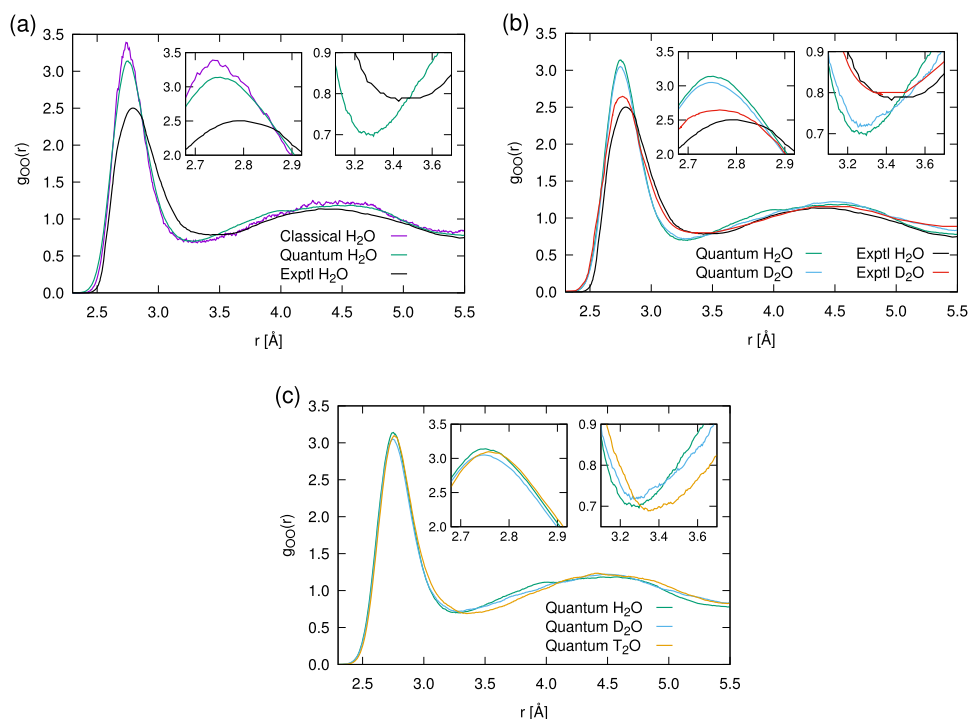


FIG. 4. Oxygen-oxygen radial distributions of liquid water. (a) The results of the classical (violet) and quantum (green) simulations of H₂O and the experimental result (black) from Ref. 52. (b) Results of the quantum simulations of H₂O (green) and D₂O (blue) and the experimental results of H₂O (black) from Ref. 52 and D₂O (red) from Ref. 45. (c) Results of the quantum simulations of H₂O (green), D₂O (blue), and T₂O (orange).

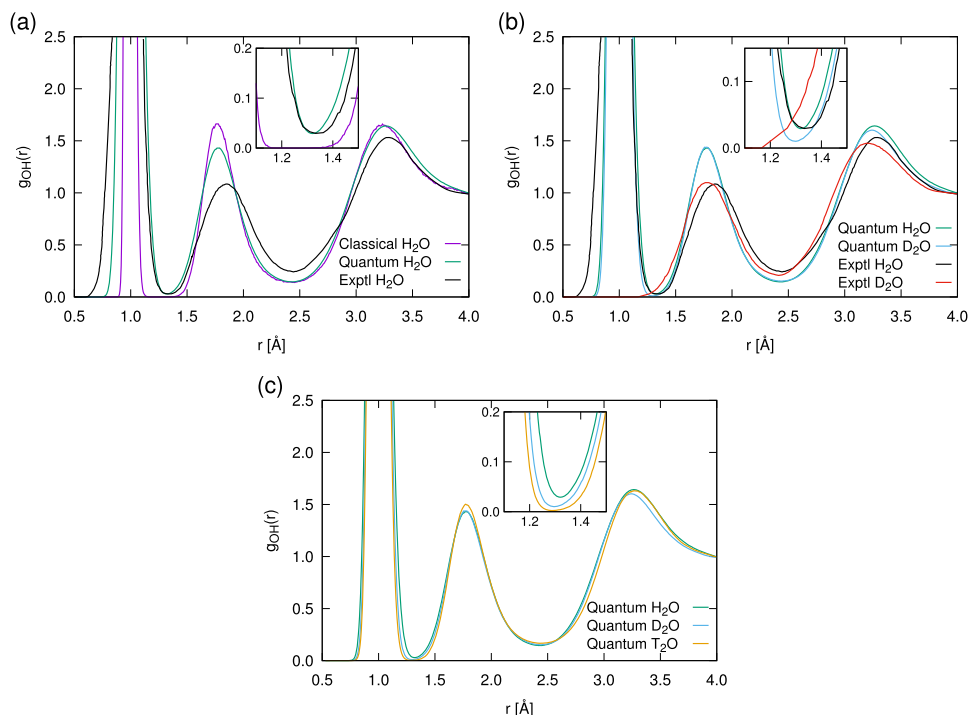


FIG. 5. Oxygen-hydrogen radial distributions of liquid water. (a) Results of the classical (violet) and quantum (green) simulations of H_2O and the experimental result (black) from Ref. 51. (b) Results of the quantum simulations of H_2O (green) and D_2O (blue) and the experimental results of H_2O (black) from Ref. 51 and D_2O (red) from Ref. 45. (c) Results of the quantum simulations of H_2O (green), D_2O (blue), and T_2O (orange).

radial distribution found in the classical simulation is due to the overstructuring of the hydrogen bonds. This is significantly improved in the quantum simulations as the quantum fluctuations induce structural disordering, but the discrepancy still remains between the simulations and the experiments. This is presumably due to the limitation of the BLYP-D2 density functional since it tends to overestimate the hydrogen bond strength as discussed above for the evaporation energy.

Nevertheless the radial distributions from the quantum simulations resemble those from experiments in many ways with respect to the isotope shift between H_2O and D_2O except

for the oxygen-oxygen first peak. Upon deuteration, the peak heights for the first peak of the oxygen-oxygen radial distribution are slightly shortened, which is the same tendency as seen in Ref. 21. However, this is not consistent with the experimental observation.⁴⁵ Here, it should be noted that even the present calculation taking into account NQE with D2 correction cannot reproduce the experimental observation. This delicate inconsistency might be improved by the use of more elaborate exchange-correlation functionals such as the hybrid functionals.^{19,20} However, such a PIMD calculation will require a huge computational effort, especially in the present

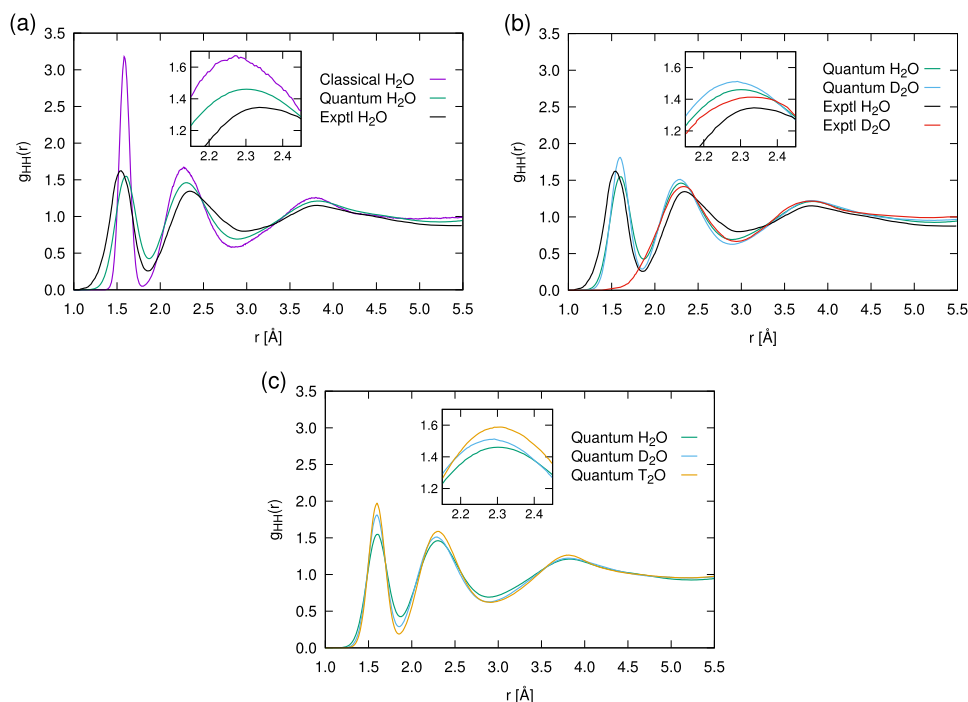


FIG. 6. Hydrogen-hydrogen radial distributions of liquid water. (a) Results of the classical (violet) and quantum (green) simulations of H_2O and the experimental result (black) from Ref. 51. (b) Results of the quantum simulations of H_2O (green) and D_2O (blue) and the experimental results of H_2O (black) from Ref. 51 and D_2O (red) from Ref. 45. (c) Results of the quantum simulations of H_2O (green), D_2O (blue), and T_2O (orange).

TABLE II. The peaks in the radial distributions of liquid water.^a

Pair	Peak		Expt. ^b		Quantum ^c			Classical ^c
	Number	Value ^d	H ₂ O	D ₂ O	H ₂ O	D ₂ O	T ₂ O	H ₂ O
OO	1	<i>r</i>	2.80	2.76	2.75 ± 0.01	2.75 ± 0.00	2.76 ± 0.01	2.74 ± 0.02
	1	<i>h</i>	2.50	2.62	3.14 ± 0.02	3.05 ± 0.06	3.10 ± 0.02	3.38 ± 0.06
OH	2	<i>r</i>	1.85	1.77	1.78 ± 0.02	1.77 ± 0.01	1.77 ± 0.01	1.76 ± 0.01
	2	<i>h</i>	1.09	1.10	1.43 ± 0.01	1.44 ± 0.04	1.50 ± 0.03	1.66 ± 0.06
	3	<i>r</i>	3.27	3.20	3.28 ± 0.02	3.24 ± 0.02	3.27 ± 0.00	3.23 ± 0.00
	3	<i>h</i>	1.53	1.48	1.64 ± 0.01	1.60 ± 0.02	1.63 ± 0.01	1.65 ± 0.02
HH	1	<i>r</i>	1.62	...	1.61 ± 0.00	1.60 ± 0.00	1.60 ± 0.00	1.58 ± 0.01
	1	<i>h</i>	1.54	...	1.55 ± 0.01	1.81 ± 0.01	1.97 ± 0.01	3.16 ± 0.03
	2	<i>r</i>	2.34	2.33	2.31 ± 0.02	2.29 ± 0.01	2.30 ± 0.01	2.26 ± 0.00
	2	<i>h</i>	1.35	1.41	1.46 ± 0.01	1.51 ± 0.03	1.59 ± 0.02	1.66 ± 0.03
	3	<i>r</i>	3.81	3.84	3.81 ± 0.02	3.81 ± 0.01	3.82 ± 0.02	3.75 ± 0.00
	3	<i>h</i>	1.15	1.21	1.21 ± 0.01	1.22 ± 0.02	1.26 ± 0.02	1.26 ± 0.00

^aIf the error is represented as all digits being filled with zero, e.g., 0.00, it means that the error is less than the reported precision.

^bData interpolated from Refs. 45, 51, and 52.

^cThis work.

^dThe peak position *r* in Å, and the peak height *h*.

calculation scheme employing the all-electron PAW scheme and the explicit imaginary-time representation based on Suzuki-Trotter expansion. On the other hand, the third peak of the oxygen-hydrogen radial distribution and the second peak of the hydrogen-hydrogen radial distribution are slightly shortened in agreement with the experimental observation. Meanwhile the second peak of the oxygen-hydrogen radial distribution does not shift significantly.

Taking a closer look at the OH radial distribution, it is interesting that the distribution in the quantum simulation does not have a region with completely zero values between the first and second peaks. Then, in order of OH, OD, and OT, the radial distributions in the quantum simulations approach zero between the first and second peaks. On the other hand, the OH radial distribution in the classical simulations has a wide zero-valued region as well. This implies that fluctuating OH bonds can stretch nearly up to the dissociative region in the presence of the nuclear quantum effect. The OH bond fluctuation can be mainly ascribed to the large zero-point vibration of OH bonds. The OD and OT bonds do not so frequently approach to the dissociative region such as OH as their zero-point vibration is not as large as that of OH bonds. This can be seen more clearly from a distribution defined with respect to the difference in the oxygen-hydrogen distances, δ , for the hydrogen bonded pairs (Fig. 7). In the quantum simulation of H₂O, the distribution is not zero at $\delta = 0$, which means that the probability of finding H atom in the middle of two oxygens is finite. In the cases of D₂O and T₂O, such a probability clearly decreases. This result was also found in the earlier studies in which quantum and classical simulations were compared,^{19,53} but the difference among the isotopologs is revealed for the first time in this study.

E. Hydrogen bond analysis

Now we analyze the hydrogen bonding in more detail. In Figs. 8 and 9, we show the two-dimensional distributions of the OH bond distance against the oxygen-oxygen distance and the O···O–H angle, respectively, for pairs of

hydrogen-bonded molecules in liquid water. In the classical simulations, we find a clear correlation between the OH bond distance and the oxygen-oxygen distance [Fig. 8(a)] as well as the O···O–H angle [Fig. 9(a)]. We can consider the hydrogen bond fluctuation relevant to the hydrogen bond strength in the following way. As the OH bond is stretched, the oxygen-oxygen distance is shortened and the O···O–H angle is closer to linear, thus trying to strengthen the hydrogen bond. On the other hand, when the OH bond is compressed, the oxygen-oxygen distance is extended and the O···O–H angle deviates from being linear, thus trying to weaken the hydrogen bond. This clearly means that OH bond stretching and its orthogonal motion bring about strengthening and weakening of the hydrogen bonding, respectively, i.e., these fluctuations compete with each other on hydrogen bonding strength. In the quantum simulations, both of these correlations still remain. This finding is consistent with what has been suggested before as the “competing quantum effects.”⁷⁹ However, the strength of correlation is dependent on the isotopologs. Among the quantum simulations, it was found that the correlation is the strongest for

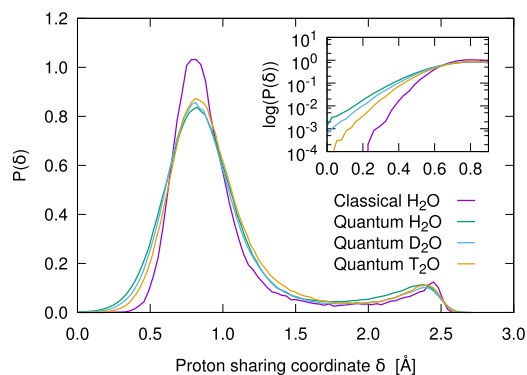


FIG. 7. Distributions of the proton sharing coordinate, $\delta = |r_{\text{O}\cdots\text{H}} - r_{\text{O-H}}|$, of hydrogen-bonded pair of water molecules. Results are shown for the classical simulation of H₂O (violet) and the quantum simulations of H₂O (green), D₂O (blue), and T₂O (orange).

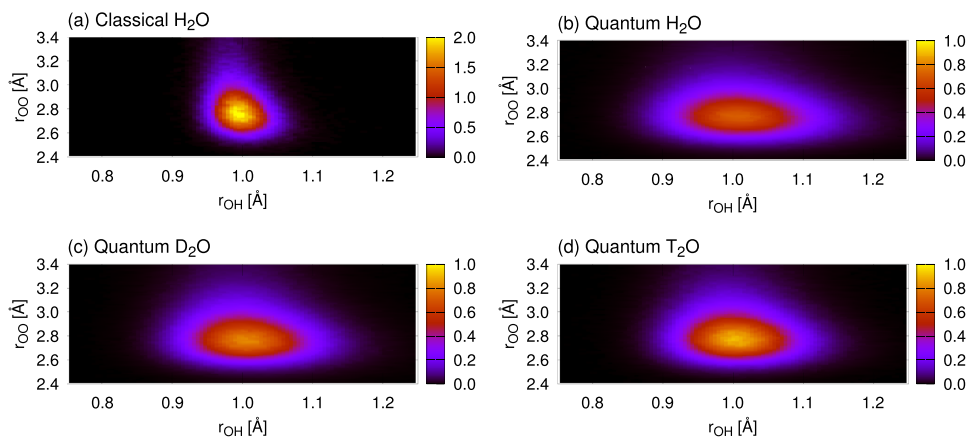


FIG. 8. Two dimensional distributions of the intramolecular OH distance of the hydrogen bond, r_{OH} , and the intermolecular $O \cdots O$ distance, $r_{O \cdots O}$, for pairs of hydrogen bonded molecules in liquid water. Results are shown for (a) the classical simulation of H_2O and (b) the quantum simulations of H_2O , (c) D_2O , and (d) T_2O .

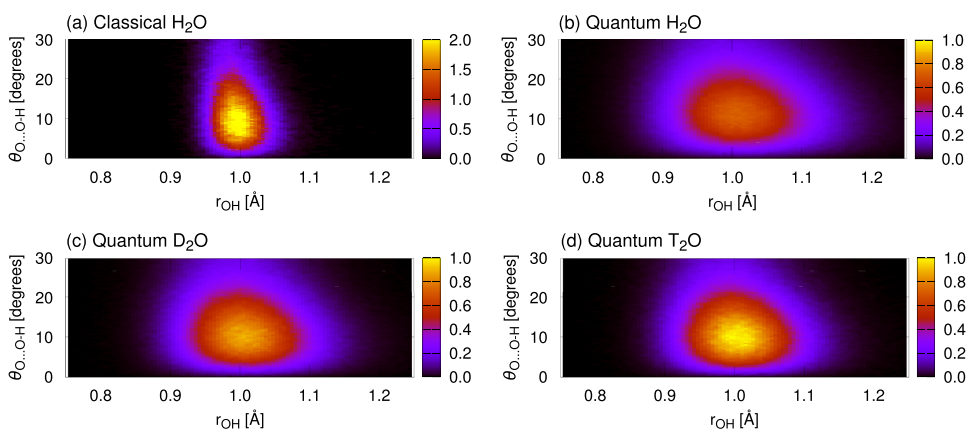


FIG. 9. Two dimensional distributions of the intramolecular OH distance of the hydrogen bond, r_{OH} , and the intermolecular $O \cdots H-O$ angle, $\theta_{O \cdots H-O}$, for pairs of hydrogen bonded molecules in liquid water. Results are shown for (a) the classical simulation of H_2O and (b) the quantum simulations of H_2O , (c) D_2O , and (d) T_2O .

T_2O , followed by D_2O and H_2O . On the other hand, the two-dimensional distributions are significantly “blurred,” and the blurred effect is the strongest for H_2O , followed by D_2O and T_2O .

F. Effects of dispersion correction

Finally it is interesting from the theoretical point of view to study the influence of the dispersion correction of DFT on the structure of water. For this purpose, the oxygen-oxygen, oxygen-hydrogen, and hydrogen-hydrogen radial distributions

were compared between those obtained from quantum simulations with and without the dispersion correction (Figs. 10–12). When the dispersion correction is absent from the classical simulation, the undulation of the radial distributions becomes greater showing the over-structured behavior (figure not shown). As was pointed out in previous literatures,^{9,13,14,25–28} this feature can be explained by the nature of attractive van der Waals interactions to stabilize water molecules in the interstitial location between the first and second hydration shells (see, e.g., Ref. 2). Figure 10 implies that the nuclear quantum effect also helps stabilize the interstitial

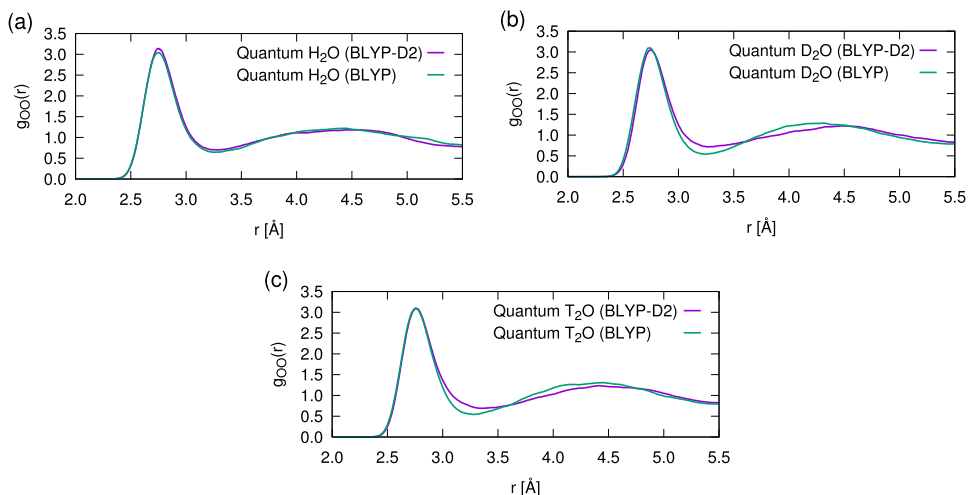


FIG. 10. Oxygen-oxygen radial distributions from the quantum simulations of liquid (a) H_2O , (b) D_2O , and (c) T_2O . Results are shown for the BLYP-D2 functional (violet) and the BLYP functional (green).

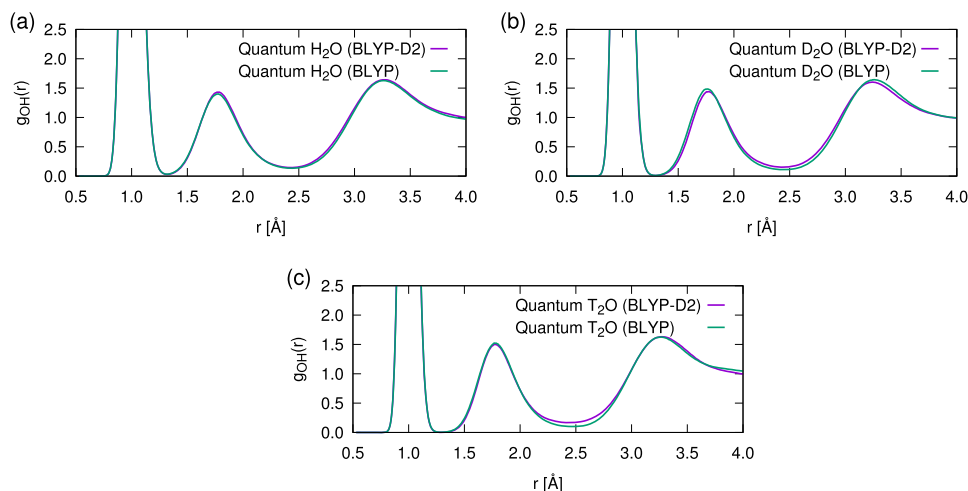


FIG. 11. Oxygen-hydrogen radial distributions from the quantum simulations of liquid (a) H_2O , (b) D_2O , and (c) T_2O . Results are shown for the BLYP-D2 functional (violet) and the BLYP functional (green).

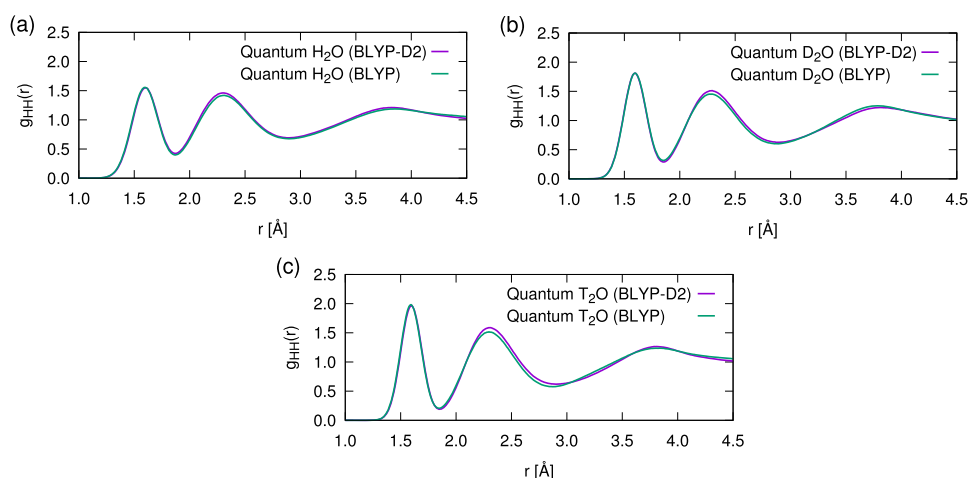


FIG. 12. Hydrogen-hydrogen radial distributions from the quantum simulations of liquid (a) H_2O , (b) D_2O , and (c) T_2O . Results are shown for the BLYP-D2 functional (violet) and the BLYP functional (green).

water molecules in a similar way. However a new finding here is that the dispersion correction and the nuclear quantum effect both correct the overstructuring, but they do not act necessarily in an additive manner. In the quantum simulations, the overstructuring in the absence of the dispersion correction is not serious for H_2O , at least for the present Grimme's D2 type. Meanwhile the dispersion correction remains important for D_2O and T_2O . Thus the dispersion correction acts differently among the isotopologs depending on the degree of structural distortions induced by quantum fluctuations. We can therefore conclude that the dispersion correction has a substantial influence only on the heavier isotopes of water. Actually we find that the oxygen-oxygen radial distributions with the dispersion correction are in better agreement compared to those without the dispersion correction in H_2O , but not in D_2O and T_2O . The oxygen-hydrogen and hydrogen-hydrogen radial distributions shown in Figs. 11 and 12 are quite similar to one another between those with and without the dispersion correction in H_2O . Although not as surprising, this confirms that the dispersion correction is not so important for hydrogen atoms.

IV. CONCLUSION

We carried out first principles PIMD simulations to study the structures of light and heavy water. The simulations were

based on all-electron calculations, and the nuclear quantum effect was fully taken into account by the second-order Suzuki-Trotter expansion. We found a systematic change in the hydrogen bond between liquid H_2O , D_2O , and T_2O . The structural fluctuations and the strength of hydrogen bonds change according to the nuclear quantum effect. It is encouraging that most of the simulation results are in reasonable agreement with available experimental data on isotope effects. In particular, the radial distributions of D_2O were found to be slightly lower for the following peaks compared with the ones for H_2O : the second peak of the hydrogen-hydrogen radial distribution and the third peak of the oxygen-hydrogen radial distribution. The D_2O evaporation energy is slightly higher than the H_2O counterpart by 0.36 kcal/mol, implying that the hydrogen bond is slightly stronger in D_2O than in H_2O . For quantitative estimation of isotope effects, the inclusion of the dispersion correction of density functionals is required. This is because the dispersion correction and the nuclear quantum effect both induce hydrogen bond fluctuations, but they do not work in an additive manner. The quantum fluctuations in H_2O fully cover the disordering induced by the dispersion correction, but do not do so fully for D_2O and T_2O .

The quantum simulations predict that the oxygen-hydrogen radial distribution of H_2O is non-zero between the first and the second peaks. Meanwhile the corresponding

distributions in D₂O and T₂O approach zero as the mass becomes heavier. Due to large quantum fluctuations, the H atoms in the OH bonds can access the dissociative region up to the hydrogen bond center, O···H···O, whereas the D (T) atoms in the OD (OT) bonds are less able to access this region.

The present quantum simulations were useful in exploring the isotope effect, and the differences among H₂O, D₂O, and T₂O. However agreement with experiment was not perfect for each system, presumably due to the density functionals employed in this work having the tendency to overestimate the hydrogen bond strength. A more reliable simulation would be *ab initio* PIMD simulations method based on the post Hartree-Fock theory, which have been already used for hydrogen bonded molecules and molecular clusters.^{80–82} Technical advances in computational efficiency will assist in conducting such completely parameter-free and accurate simulations of the condensed phases.

ACKNOWLEDGMENTS

The simulations were performed on FUJITSU PRIMERGY BX900 and SGI ICE X supercomputers in CCSE JAEA. The authors thank CCSE staff members for their support. M.S. thanks the support from JSPS KAKENHI Grant No. 16K05675. M.M. also thanks the support from JSPS KAKENHI Grant Nos. 16H04624, 16H02450, 16H02437, and 15K00718. M.M. is indebted to K. Sakuramoto and H. Nakamura for their technical support in using VASP. All authors are grateful to Dr. A. Malins in JAEA for proofreading the manuscript of this paper.

- ¹M. Ceriotti, W. Fang, P. G. Kusalik, R. H. McKenzie, A. Michaelides, M. A. Morales, and T. E. Markland, *Chem. Rev.* **116**, 7529 (2016).
- ²M. J. Gillan, D. Alfè, and A. Michaelides, *J. Chem. Phys.* **144**, 130901 (2016).
- ³M. Sprik, J. Hutter, and M. Parrinello, *J. Chem. Phys.* **105**, 1142 (1996).
- ⁴S. Izvekov and G. A. Voth, *J. Chem. Phys.* **116**, 10372 (2002).
- ⁵J. C. Grossman, E. Schwegler, E. W. Draeger, F. Gygi, and G. Galli, *J. Chem. Phys.* **120**, 300 (2004).
- ⁶J. VandeVondele, F. Mohamed, M. Krack, J. Hutter, M. Sprik, and M. Parrinello, *J. Chem. Phys.* **122**, 014515 (2005).
- ⁷P.-L. Sit and N. Marzari, *J. Chem. Phys.* **122**, 204510 (2005).
- ⁸H.-S. Lee and M. E. Tuckerman, *J. Chem. Phys.* **126**, 164501 (2007).
- ⁹J. Schmidt, J. VandeVondele, I.-F. W. Kuo, D. Sebastiani, J. I. Siepmann, J. Hutter, and C. J. Mundy, *J. Phys. Chem. B* **113**, 11959 (2009).
- ¹⁰G. Miceli, S. de Gironcoli, and A. Pasquarello, *J. Chem. Phys.* **142**, 034501 (2015).
- ¹¹M. Guidon, F. Schiffmann, J. Hutter, and J. VandeVondele, *J. Chem. Phys.* **128**, 214104 (2008).
- ¹²M. Guidon, J. Hutter, and J. VandeVondele, *J. Chem. Theory Comput.* **6**, 2348 (2010).
- ¹³M. Del Ben, J. Hutter, and J. VandeVondele, *J. Chem. Phys.* **143**, 054506 (2015).
- ¹⁴R. A. DiStasio, Jr, B. Santra, Z. Li, X. Wu, and R. Car, *J. Chem. Phys.* **141**, 084502 (2014).
- ¹⁵B. Santra, R. A. DiStasio, Jr, F. Martelli, and R. Car, *Mol. Phys.* **113**, 2829 (2015).
- ¹⁶A. P. Gaiduk, F. Gygi, and G. Galli, *J. Phys. Chem. Lett.* **6**, 2902 (2015).
- ¹⁷M. Del Ben, M. Schönherr, J. Hutter, and J. VandeVondele, *J. Phys. Chem. Lett.* **4**, 3753 (2013).
- ¹⁸S. Y. Willow, M. A. Salim, K. S. Kim, and S. Hirata, *Sci. Rep.* **5**, 14358 (2015).
- ¹⁹W. Chen, F. Ambrosio, G. Miceli, and A. Pasquarello, *Phys. Rev. Lett.* **117**, 186401 (2016).
- ²⁰O. Marsalek and T. E. Markland, *J. Phys. Chem. Lett.* **8**, 1545 (2017).
- ²¹B. Chen, I. Ivanov, M. L. Klein, and M. Parrinello, *Phys. Rev. Lett.* **91**, 215503 (2003).
- ²²S. Yoo, X. C. Zeng, and S. S. Xantheas, *J. Chem. Phys.* **130**, 221102 (2009).
- ²³S. Yoo and S. S. Xantheas, *J. Chem. Phys.* **134**, 121105 (2011).
- ²⁴A. P. Seitsonen and T. Bryk, *Phys. Rev. B* **94**, 184111 (2016).
- ²⁵I.-C. Lin, A. P. Seitsonen, M. D. Coutinho-Neto, I. Tavernelli, and U. Rothlisberger, *J. Phys. Chem. B* **113**, 1127 (2009).
- ²⁶J. Wang, G. Román-Pérez, J. M. Soler, E. Artacho, and M.-V. Fernández-Serra, *J. Chem. Phys.* **134**, 024516 (2011).
- ²⁷Z. Ma, Y. Zhang, and M. E. Tuckerman, *J. Chem. Phys.* **137**, 044506 (2012).
- ²⁸K. Forster-Tonigold and A. Groß, *J. Chem. Phys.* **141**, 064501 (2014).
- ²⁹C. Fang, W.-F. Li, R. S. Koster, J. Klimeš, A. Van Blaaderen, and M. A. Van Huis, *Phys. Chem. Chem. Phys.* **17**, 365 (2015).
- ³⁰S. Y. Willow, X. C. Zeng, S. S. Xantheas, K. S. Kim, and S. Hirata, *J. Phys. Chem. Lett.* **7**, 680 (2016).
- ³¹T. D. Kuhne, M. Krack, and M. Parrinello, *J. Chem. Theory Comput.* **5**, 235 (2009).
- ³²R. Z. Khaliullin and T. D. Kuhne, *Phys. Chem. Chem. Phys.* **15**, 15746 (2013).
- ³³K. Lejaeghere, G. Bihlmayer, T. Björkman, P. Blaha, S. Blügel, V. Blum, D. Caliste, I. E. Castelli, S. J. Clark, A. Dal Corso *et al.*, *Science* **351**, aad3000 (2016).
- ³⁴G. Miceli, J. Hutter, and A. Pasquarello, *J. Chem. Theory Comput.* **12**, 3456 (2016).
- ³⁵R. P. Feynman, *Statistical Mechanics: A Set of Lectures* (Hachette, UK, 1998).
- ³⁶R. P. Feynman, A. R. Hibbs, and D. F. Styer, *Quantum Mechanics and Path Integrals* (Courier Corporation, 2010).
- ³⁷D. Chandler and P. G. Wolynes, *J. Chem. Phys.* **74**, 4078 (1981).
- ³⁸M. Tuckerman, *Statistical Mechanics: Theory and Molecular Simulation* (Oxford University Press, 2010).
- ³⁹D. Marx and M. Parrinello, *J. Chem. Phys.* **104**, 4077 (1996).
- ⁴⁰D. Marx and J. Hutter, *Ab Initio Molecular Dynamics: Basic Theory and Advanced Methods* (Cambridge University Press, 2009).
- ⁴¹M. Shiga, M. Tachikawa, and S. Miura, *Chem. Phys. Lett.* **332**, 396 (2000).
- ⁴²M. Shiga, M. Tachikawa, and S. Miura, *J. Chem. Phys.* **115**, 9149 (2001).
- ⁴³F. Paesani and G. A. Voth, *J. Phys. Chem. B* **113**, 5702 (2009).
- ⁴⁴D. M. Wilkins, D. E. Manolopoulos, S. Pipolo, D. Laage, and J. T. Hynes, *J. Phys. Chem. Lett.* **8**, 2602 (2017).
- ⁴⁵A. K. Soper and C. J. Benmore, *Phys. Rev. Lett.* **101**, 065502 (2008).
- ⁴⁶J. A. Morrone and R. Car, *Phys. Rev. Lett.* **101**, 017801 (2008).
- ⁴⁷Y. Nagata, R. E. Pool, E. H. G. Backus, and M. Bonn, *Phys. Rev. Lett.* **109**, 226101 (2012).
- ⁴⁸J. Kessler, H. Elgabarty, T. Spura, K. Karhan, P. Partovi-Azar, A. A. Hassanali, and T. D. Kuhne, *J. Phys. Chem. B* **119**, 10079 (2015).
- ⁴⁹L. Wang, M. Ceriotti, and T. E. Markland, *J. Chem. Phys.* **141**, 104502 (2014).
- ⁵⁰M. Ceriotti and T. E. Markland, *J. Chem. Phys.* **138**, 014112 (2013).
- ⁵¹A. K. Soper, *Chem. Phys.* **258**, 121 (2000).
- ⁵²A. K. Soper, *ISRN Phys. Chem.* **2013**, 279463.
- ⁵³M. Ceriotti, J. Cuny, M. Parrinello, and D. E. Manolopoulos, *Proc. Natl. Acad. Sci. U. S. A.* **110**, 15591 (2013).
- ⁵⁴P. E. Blöchl, *Phys. Rev. B* **50**, 17953 (1994).
- ⁵⁵M. Lozada-Hidalgo, S. Hu, O. Marshall, A. Mishchenko, A. N. Grigorenko, R. A. W. Dryfe, B. Radha, I. V. Grigorieva, and A. K. Geim, *Science* **351**, 68 (2015).
- ⁵⁶M. Lozada-Hidalgo, S. Zhang, S. Hu, A. Esfandiari, I. Grigorieva, and A. Geim, *Nat. Commun.* **8**, 15215 (2017).
- ⁵⁷M. Shiga, PIMD version 2.0, 2016.
- ⁵⁸G. Kresse and J. Hafner, *Phys. Rev. B* **47**, 558 (1993).
- ⁵⁹G. Kresse and J. Hafner, *Phys. Rev. B* **49**, 14251 (1994).
- ⁶⁰G. Kresse and J. Furthmüller, *Comput. Mater. Sci.* **6**, 15 (1996).
- ⁶¹G. Kresse and J. Furthmüller, *Phys. Rev. B* **54**, 11169 (1996).
- ⁶²G. Kresse and D. Joubert, *Phys. Rev. B* **59**, 1758 (1999).
- ⁶³S. Ruiz-Barragan, K. Ishimura, and M. Shiga, *Chem. Phys. Lett.* **646**, 130 (2016).
- ⁶⁴A. D. Becke, *Phys. Rev. A* **38**, 3098 (1988).
- ⁶⁵C. Lee, W. Yang, and R. G. Parr, *Phys. Rev. B* **37**, 785 (1988).
- ⁶⁶S. Grimme, *J. Comput. Chem.* **27**, 1787 (2006).

- ⁶⁷G. J. Martyna, M. L. Klein, and M. Tuckerman, *J. Chem. Phys.* **97**, 2635 (1992).
- ⁶⁸W. G. Hoover, *Phys. Rev. A* **31**, 1695 (1985).
- ⁶⁹S. Nosé, *J. Chem. Phys.* **81**, 511 (1984).
- ⁷⁰W. Shinoda and M. Shiga, *Phys. Rev. E* **71**, 041204 (2005).
- ⁷¹H. A. Stern, F. Rittner, B. J. Berne, and R. A. Friesner, *J. Chem. Phys.* **115**, 2237 (2001).
- ⁷²M. E. Tuckerman, B. J. Berne, and G. J. Martyna, *J. Chem. Phys.* **97**, 1990 (1992).
- ⁷³M. E. Tuckerman, B. J. Berne, G. J. Martyna, and M. L. Klein, *J. Chem. Phys.* **99**, 2796 (1993).
- ⁷⁴A. Luzar and D. Chandler, *Nature* **379**, 55 (1996).
- ⁷⁵M. Tachikawa and M. Shiga, *J. Chem. Phys.* **121**, 5985 (2004).
- ⁷⁶M. Shiga and W. Shinoda, *J. Chem. Phys.* **123**, 134502 (2005).
- ⁷⁷K. Kuchitsu and Y. Morino, *Bull. Chem. Soc. Jpn.* **38**, 814 (1965).
- ⁷⁸D. Eisenberg and W. Kauzmann, *The Structure and Properties of Water* (Oxford University Press on Demand, 2005).
- ⁷⁹S. Habershon, T. E. Markland, and D. E. Manolopoulos, *J. Chem. Phys.* **131**, 024501 (2009).
- ⁸⁰T. Fujita, S. Tanaka, T. Fujiwara, M.-A. Kusa, Y. Mochizuki, and M. Shiga, *Comput. Theor. Chem.* **997**, 7 (2012).
- ⁸¹M. Shiga and M. Masia, *J. Chem. Phys.* **139**, 144103 (2013).
- ⁸²T. Spura, H. Elgabarty, and T. D. Kuhne, *Phys. Chem. Chem. Phys.* **17**, 14355 (2015).